Short circuit of water vapor and polluted air to the global stratosphere by convective transport over the Tibetan Plateau

Rong Fu*†, Yuanlong Hu*, Jonathon S. Wright*, Jonathan H. Jiang‡, Robert E. Dickinson*†, Mingxuan Chen*, Mark Filipiak§, William G. Read‡, Joe W. Waters‡, and Dong L. Wu‡

*School of Earth and Atmospheric Sciences, Georgia Institute of Technology, Atlanta, GA 30332-0340; ‡Jet Propulsion Laboratory, California Institute of Technology, Pasadena, CA 91109; and §Institute of Atmospheric and Environmental Science, School of Geosciences, University of Edinburgh, EH9 3JN Edinburgh, United Kingdom

Contributed by Robert E. Dickinson, February 25, 2006

During boreal summer, much of the water vapor and CO entering the global tropical stratosphere is transported over the Asian monsoon/Tibetan Plateau (TP) region. Studies have suggested that most of this transport is carried out either by tropical convection over the South Asian monsoon region or by extratropical convection over southern China. By using measurements from the newly available National Aeronautics and Space Administration Aura Microwave Limb Sounder, along with observations from the Aqua and Tropical Rainfall-Measuring Mission satellites, we establish that the TP provides the main pathway for cross-tropopause transport in this region. Tropospheric moist convection driven by elevated surface heating over the TP is deeper and detrains more water vapor, CO, and ice at the tropopause than over the monsoon area. Warmer tropopause temperatures and slower-falling, smaller cirrus cloud particles in less saturated ambient air at the tropopause also allow more water vapor to travel into the lower stratosphere over the TP, effectively short-circuiting the slower ascent of water vapor across the cold tropical tropopause over the monsoon area. Air that is high in water vapor and CO over the Asian monsoon/TP region enters the lower stratosphere primarily over the TP, and it is then transported toward the Asian monsoon area and disperses into the large-scale upward motion of the global stratospheric circulation. Thus, hydration of the global stratosphere could be especially sensitive to changes of convection over the TP.

climate | CO | stratosphere water vapor

Water vapor concentrations in the tropical lower stratosphere (LS) are 60% greater in boreal summer than in winter. This seasonal variation not only influences the radiation budget near the local tropopause but also propagates upward and toward the pole with the global stratospheric circulation (1, 2). Numerical simulations suggest that ≈75% of the total summer water vapor transport into the global tropical stratosphere may occur over the South Asian monsoon and Tibetan Plateau (TP) regions (3), contributing to >25% of the water vapor in the middle stratosphere (4).

Studies have hypothesized that an increase in cross-tropopause transport in the Asian monsoon/TP region may have contributed to an increasing trend in stratospheric water vapor (5) during the 1980s and 1990s (6, 7). This trend probably increased the global greenhouse forcing (8) and enhanced ozone depletion in the Arctic (9). Any explanation of this trend or future trends would likely need to address how source regions for stratospheric water have changed. Recent studies have revealed high CO in the upper troposphere (UT) over the South Asian monsoon region (10). This CO is produced by biomass or fossil fuel burning, suggesting a human influence on transport of combustion pollutants and, perhaps, water vapor into the LS (11). Thus, a clarification of the mechanisms of water vapor and CO transport into the LS in this region is an important step toward understanding tropospheric influences on hydration and chemical composition in the global stratosphere.

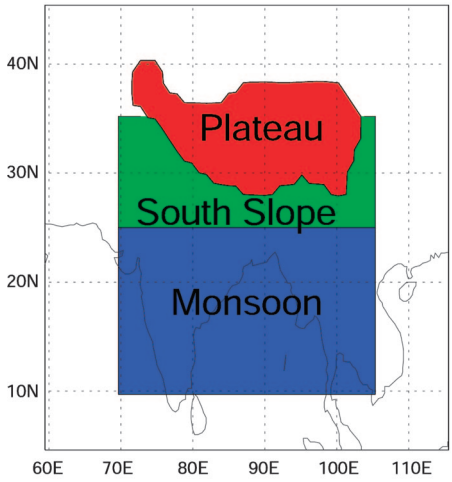

Fig. 1. Regions defined in this study. The TP is defined as the area with an elevation of >3 km within 70–105°E and 25–40°N, the Plateau south slope is defined as the area with elevation <3 km within 70–105°E and 25–35°N, and the monsoon area is defined as 70–105°E, 10–25°N.

Deep convection (i.e., thunderstorm updrafts) occurs most frequently over the Bay of Bengal and Indian subcontinent, which are collectively referred to as the South Asian monsoon region (Fig. 1), or simply the monsoon region. Studies (7, 10, 12) have suggested that transport by monsoon convection produces large concentrations of water vapor and CO and lower concentrations of ozone in the UT; however, the highest water vapor concentrations in the LS (e.g., 100 hPa at ≈18 km above sea level) are located north of the monsoon region (13), primarily over the TP and its south slope (Fig. 1). To explain the northward displacement of the LS hydration center away from the monsoon region, it has been proposed that water vapor is transported by monsoon convection to the UT and then sometimes transported northward isentropically to the extratropical tropopause break north of the TP (14). However, such irreversible isentropic transport may be limited because of a strong anticyclonic

Conflict of interest statement: No conflicts declared.

Abbreviations: AIRS, Atmospheric Infrared Sounder; IWC, ice-water content; LS, lower stratosphere; MLS, Microwave Limb Sounder; MODIS, Moderate-Resolution Imaging Spectroradiometer; NASA, National Aeronautics and Space Administration; PR, precipitation radar; RH, relative humidity; TP, Tibetan Plateau; TRMM, Tropical Rainfall Measuring Mission; UT, upper troposphere; ppbv, parts per billion by volume.

†To whom correspondence may be addressed. E-mail: fu@eas.gatech.edu or robted@eas.gatech.edu.

www.pnas.org/cgi/doi/10.1073/pnas.0601584103

circulation over the TP (15). This transport would take a few weeks (12), exposing the air to recurrent cold-temperature anomalies that reduce humidity to below the large-scale average saturation (16). An alternative explanation is that extratropical convection allows water vapor to bypass the cold tropical tropopause (3, 17). Water vapor entering the extratropical LS, especially in southern China, can travel toward the equator into the tropical LS (3, 18). None of the studies described above account for the maximum of water vapor over the TP; therefore, the following two aspects remain unclear: whether the aforementioned isentropic cross-tropopause transport could account for the LS water vapor maximum north of the monsoon convection or, alternatively, whether local convection provides the main contribution to the LS hydration center over the TP.

The TP is located north of the monsoon region, covering an area that is approximately half the area of the lower 48 states in the United States, with an average elevation of >4 km. Satellite surveys show that clouds indicating deep moist convection occur frequently over the eastern Plateau (19). Because of low air density and strong surface heating over the TP, air is mixed up to ≈8 km above sea level (20) by dry thermal updrafts. Convergence in the lower and middle troposphere resulting from the surface heating and rising air draws water vapor and pollution from the monsoon region (21, 22). Over the TP in summer the altitude of the tropopause, defined as where potential temperature reaches 380 K (23), is generally located near 17 km above sea level (≈105 hPa). Potential temperature is an indicator of the internal and potential energy of the atmosphere. Higher values of potential temperature and humidity for near surface air increase the probability of air rising from the surface to convect to the UT.

The potential temperature of air near surface over the TP can often be 30–40 K warmer than those over the monsoon area, and, thus, much lower humidities are necessary for moist convection to carry surface air parcels to the tropopause. The high elevation of the TP approximately halves both the depth of the tropospheric column and the total water vapor relative to the monsoon area, allowing more upwelling infrared radiation from the surface to reach and warm the tropopause. This article proposes that convection and atmospheric circulation over the TP represent the primary transport pathway of water vapor and CO to the LS. We explored this hypothesis by using measurements from the Aura Microwave Limb Sounder (MLS), Aqua Moderate-Resolution Imaging Spectroradiometer (MODIS), and Atmospheric Infrared Sounder (AIRS), and Tropical Rainfall Measuring Mission (TRMM) precipitation radar (PR). The Aura satellite was launched by the National Aeronautics and Space Administration (NASA) on July 15, 2004, to join the Aqua satellite in the "A-train." The two satellites view the same location within 7 min, which is shorter than the lifetime of individual mesoscale convective systems. This unprecedented match in space and time enables us to determine more accurately the influence of convection on cirrus cloud microphysical properties, water vapor, and polluted air in the UT/LS.

Results and Discussion

This study addresses whether more water vapor and CO are transported into the LS by convection over the TP than over the monsoon region. We examined whether the tropopause is warmer, whether convection is deeper and injects more water vapor and CO to the tropopause, and whether water vapor and CO in the LS originate mostly from the TP or in the monsoon region. Fig. 2 shows the distribution of convective tops that reach >10 km altitude in August 2004 and 2005, where the convective top is defined as the highest level at which TRMM PR rain rate is >0.5 mm/h, which is the lowest detectable rain rate by the instrument. The deeper convection (particularly with a convective top of >14 km) occurs more frequently over the TP and the

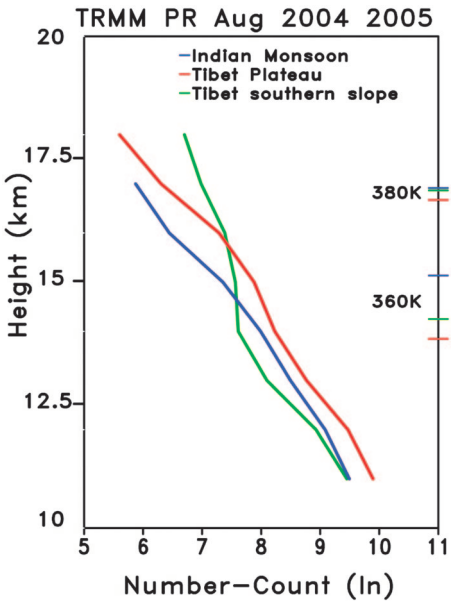

Fig. 2. Number counts of convective tops >10 km as a function of altitude over the TP (red), Plateau south slope (green), and monsoon region (blue) during the period of August 2004 and 2005 derived from TRMM PR rain rate (product 2A25). The tropopause (380 K) and 360 K in these three regions are indicated on the right axis with the same color as defined for the profiles.

Plateau south slope than over the monsoon region. The level of 14 km corresponds to 360 K and is the level over the TP above which radiative heating is positive such that water and CO detrained from convection can rise spontaneously (24). MLS ice-water content (IWC) similarly indicates that the frequency of cirrus/anvil clouds reaching the tropopause is much greater over the TP (71%) and the Plateau south slope (86%) than over the monsoon area (25%). The mean cirrus/anvil cloud top pressure as indicated by AIRS data is 150 hPa (14 km in altitude) over the TP, compared with 300 hPa (9 km) over the monsoon area. Therefore, the results from these three satellites consistently suggest that the overshooting of water vapor and ice into the overlying stable air is deeper over the TP and its south slope than over the monsoon region. Deeper convection over the TP does not necessarily produce more rainfall at the surface, because of its unusually high convective base and low ambient humidity, which reduce the amount of water vapor that is entrained into the convective tower and, consequently, rainfall.

Convection can transport both CO and water vapor from surface sources to the UT or LS, where they are further transported vertically and horizontally by the large-scale circulation. The transport of both constituents is determined by near-surface concentrations and convective mass transport within their lifetimes (≈1 month for CO and approximately a few days for water vapor), whereas the transport of water vapor is additionally controlled by atmospheric temperature. Thus, we first examined the CO transport, which is more closely related to the convective mass transport. The occurrence of CO vertical transport by convection can be diagnosed observationally by comparing increased concentrations of CO in the presence of convection with the background CO. Fig. 3 shows that CO between 215 (≈12 km) and 100 hPa, referred to as the tropopause layer (25), increases as much with convection over the TP and Plateau south slope as over the monsoon area. Thus, convective mass transport over the TP and Plateau south slope must be stronger than over the monsoon area, because near-surface CO over these areas is less than half of that over the monsoon area. This implied stronger convective transport is

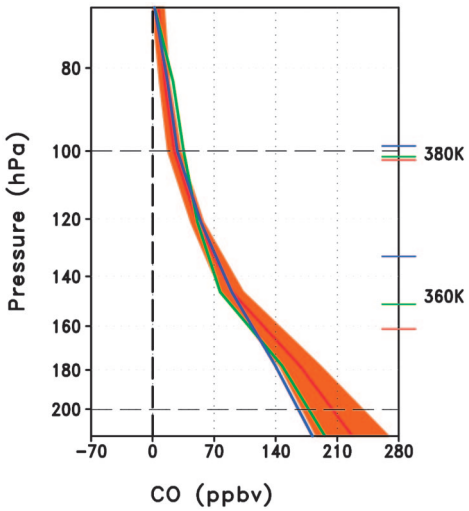

Fig. 3. Profiles of the change of CO mixing ratio between deep convection and clear sky for the TP (red), Plateau south slope (green), and monsoon area (blue) as derived from the MLS. Deep convection is defined by the presence of IWC at two or more consecutive pressure levels >215 hPa and with the cloud top reaching ≥147 hPa. Shade indicates the 90% confidence range for the TP. The tropopause (380 K) and 360 K in these three regions are marked on the right axis with the same color as defined for the profiles.

consistent with the deeper convective tops shown in Fig. 2. The concentration of CO decreases with altitude, consistent with successively fewer convective tops occurring at higher elevations (Fig. 2).

Previous numerical modeling has indicated that monsoon convection may dominate transport of CO to the UT (10). We examined this suggestion observationally. Fig. 4*a* shows that the center of high 100-hPa MLS CO [>80 parts per billion by volume (ppbv)] over the northern monsoon, Plateau south slope, and southern TP area is located at 20–30°N. This high-CO air was traced back to the vicinity of the TP 5 days earlier by a back-trajectory analysis (Fig. 4*b*) and remained in that region for the previous 2 weeks (Fig. 4*c*). Figs. 2 and 4 suggest that a significant fraction of the high CO throughout the region must have ascended to the LS over the TP and its south slope and followed the upper-level anticyclonic flow at the core of the Tibetan High (Fig. 4 *b* and *c*). Trajectory analysis for high CO observed at 147 hPa (> 140 ppbv) also suggests that it originates primarily from the TP. In contrast, most CO transported to the tropopause layer by monsoon convection is carried away by the easterly winds (Fig. 4 *b* and *c*) rather than contributing to the high-CO center in the Asian monsoon/TP region.

Excess LS water vapor observations (> 5 ppmv at 100 hPa) are concentrated more over the TP than those of high CO (Figs. 4*a* and 5*a*). We applied a separate back-trajectory analysis to determine the source region of the high-MLS water-vapor mixing ratios over the whole Asian monsoon/TP region. Water vapor that was detrained from convection was typically depleted in ≈1 day (26). The primary convective source should be located along the back trajectories within the previous few days. Apparently, much of the moist air was either transported upward by local convection in the Plateau south slope and southeastern TP (Fig. 5*a*) or horizontally by large-scale flow from the central and eastern TP (Fig. 5 *b* and *c*), suggesting that the hydrated air first rises to the LS in the TP and its south slope (Fig. 5 *b* and *c*), then is transported southward toward the monsoon area (Fig. 5*a*), the same path as for CO. This transport toward the equator is consistent with inferences of studies (3, 18) using monthly mean data and numerical simulations. Quantitatively, ≈35–40% of the air with excess water vapor comes from the TP, 12–22% comes from the Plateau south slope, <10% comes from the monsoon area, and the rest comes from other areas in Asia.

We then sought to determine why more LS water vapor comes from the TP rather than the monsoon region. Fig. 6 shows that the water vapor mixing ratio in the tropopause layer increases more than twice as much with convection over the TP and Plateau south slope, as it does over the monsoon region, indicating a greater moistening effect by convection over the TP. MLS data indicate that the mean clear sky temperature of the tropopause layer over the TP is 7–8 K warmer than over the monsoon area. This temperature difference translates to at least a 2.5 times larger saturated mixing ratio (i.e., an additional 7–8 ppmv in the tropopause layer over the TP than over the monsoon area). Thus, less water vapor would be condensed out over the TP than over the monsoon area. Ambient relative humidity (RH) and cloud-particle sizes can also influence the convective moistening effect (17, 27, 28). Very deep convection observed over the TP can overshoot and detrain ice particles near or even above the tropopause. Smaller ice particles can reach higher altitudes and fall at slower speed. The sublimation of these ice particles in ambient air can further moisten the tropopause and LS even after the dissipation of their convective source. The MLS shows that ambient RH with respect to ice (RH_i) is <40% at the tropopause over the TP, compared with >70% over the monsoon area. The MODIS also indicates a 10% greater fraction of the smaller ice particles (bin, 20–25 μm) and 5% less of the

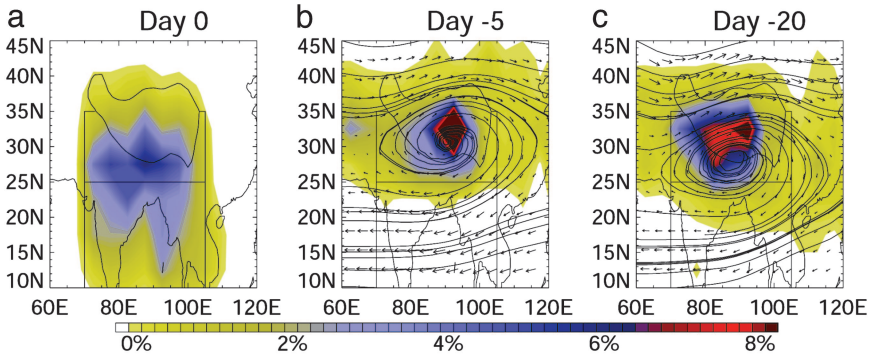

Fig. 4. Relative concentration of high-CO samples (>80 ppbv) per 2.5° latitude by 3.75° longitude box (≈10^5 km^2) at 100 hPa (*a*) as derived from 939 samples that were measured by MLS during August 2004 and 2005 5 days (*b*) and 20 days (*c*) previously as determined by the back-trajectories of the high-CO samples shown in *a*. The vectors and lines in *b* indicate the horizontal wind and streamlines, respectively, at 100 hPa averaged over the period of August 2004 and 2005. Based on the ascending velocity in this region, high-CO air shown in *a* could be located near 200 hPa 20 days previously. The directions in which it would be carried are indicated by the horizontal wind and streamlines at 200 hPa in *c*.

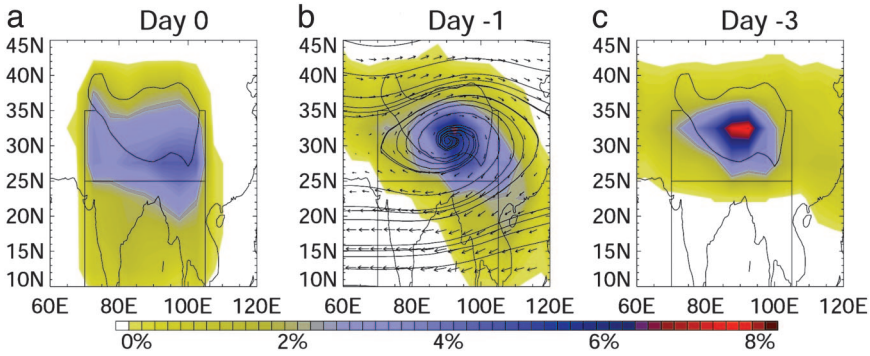

Fig. 5. Relative concentration of high-water vapor samples (>5 ppmv) per 2.5° latitude by 3.75° longitude box (≈10^5 km^2) at 100 hPa (*a*) derived from 1,022 samples that were measured by MLS during August 2004 and 2005 1 day (*b*) and 3 days (*c*) previously as determined by the back-trajectories of the high-water vapor samples that are shown in *a*. The vectors and lines in *b* indicate the horizontal wind and streamlines, respectively, at 100 hPa averaged over the period of August 2004 and 2005. Because of the relatively short time scale of these integrations, the 200-hPa wind is not shown in this case.

bigger particles (bin, 25–35 μm) at the top of cirrus/anvil clouds for unpolluted atmosphere (aerosol optical depth, <0.2) over the TP than over the monsoon area (Fig. 7). This shift toward smaller particles is consistent with the higher convective and cirrus/anvil tops over the TP. Thus, smaller ice particles that are overshot by convection into a less saturated tropopause may also contribute to the stronger hydration of the tropopause and LS over the TP. Over the Plateau south slope, the tropopause temperature is 4–5 K colder and RH_i is 20% higher than over the TP. Thus, the cross-tropopause water vapor transport over that region is probably weaker than it is over the TP (Fig. 6), despite the presence of comparable convection.

Ref. 12 has shown a higher water vapor concentration of <215 hPa in the monsoon region that would travel to the tropopause over a few weeks (29) and, thus, would be freeze-dried by recurrent cold-temperature anomalies (16). In contrast, Figs. 6 and 7 show that deeper convection over the TP transports water vapor and smaller ice particles to a warmer and less saturated tropopause over the TP, short-circuiting the cold tropopause barrier for water vapor transport that exists in the monsoon and other tropical regions. Thus, convection over the TP provides the main pathway for water entering the LS in the Asian monsoon/TP region. Because water vapor depletes much faster than CO during transport toward the monsoon area, the LS center of hydration is more localized over the TP than that of high CO.

We then questioned what the likely importance of isentropic transport of water vapor and CO across the tropopause break at 40°N is, as emphasized in refs. 14 and 17, relative to the convective transport described above. Figs. 4 and 5 indicate that the probability of the isentropic path they propose is much lower. Rather, these images suggest that air that is rich in water vapor and CO injected into the LS over the TP travels toward the equator toward the monsoon-area (ref. 4; Figs. 4 *a* and *b* and 5 *a* and *b*), where it can mix into tropical LS air and participate in the large-scale tropical rising motion of the global stratospheric circulation (2, 18).

Evidently, the hydration of the global stratosphere could be especially sensitive to natural and human-induced climate change over the TP, especially the observed warming of surface temperatures (30). This conclusion highlights the need to monitor these changes and their impacts more closely. In particular, establishing how these changes would alter the composition of the stratosphere, especially water, could help ascertain the influence of local tropospheric climate change on changes of the global stratosphere. It is possible that Aura and other satellites

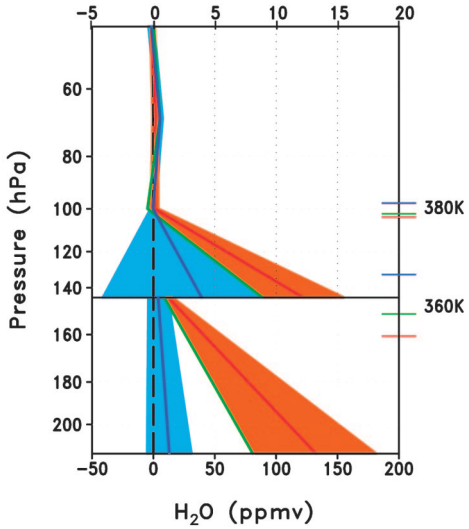

Fig. 6. As in Fig. 3, but for the change of H_2O mixing ratio between deep convection and clear sky as derived from MLS data. The 90% confidence range is shaded for the TP and monsoon area. Deep convection is as defined in Fig. 3. The *x*-axis scales differ for profiles <147 hPa in *Lower* and >120 hPa in *Upper*.

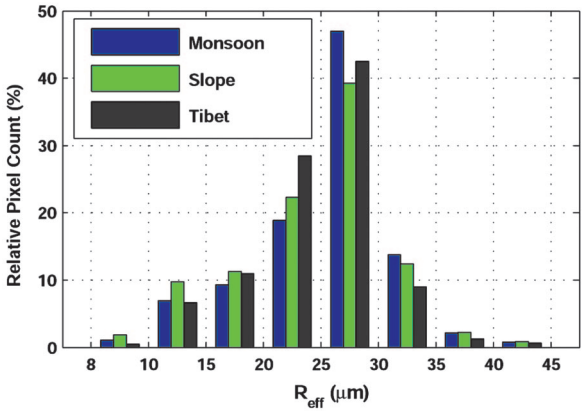

Fig. 7. Fraction of ice particles at the tops of cirrus/anvil clouds for each size bin relative to the total number of cirrus particles that were derived from MODIS under unpolluted conditions (aerosol optical depth, <0.2) for the three areas. Cirrus-particle sizes were obtained from Aqua MODIS for cloud tops of >200 hPa. Samples range from a minimum of 200 pixels to a maximum of 670,000 pixels for each particle-size bin.

GEOPHYSICS

in the A-train constellation will provide highly valuable information to address these issues.

Methods

The Aura MLS simultaneously measures water vapor, cloud ice, temperature, and CO, as well as other chemical tracers, on fixed-pressure surfaces between 80°N and 80°S (31). This study used instantaneous along-track profiles of water vapor, CO, temperature, and IWC measured by the MLS. For water vapor, the MLS single-measurement precision varies between ≈25% (at 316 hPa) and ≈10% (at 100 hPa), with an estimated accuracy of ≈10%; for CO, the single-measurement precision is ≈25%, with an estimated accuracy of >30% above 147 hPa (32). The IWC single-measurement sensitivity is ≈4 mg·m^{-3} at 215 hPa and 0.4 mg·m^{-3} at 147 and 100 hPa. MLS cannot detect thin cirrus below the instrument sensitivity, and, thus, the thicker cirrus/anvil detectable by MLS are produced mostly by convective detrainment. MLS may underestimate cloud IWC by more than ≈50 mg·m^{-3} because of saturation in the ice signal. Such underestimation is estimated to be <15% of total ice mass at 215 hPa and <5% at 147 hPa and higher levels (33).

The vertical structure of convection is inferred from the TRMM PR (34) 2A25 algorithm volumetric radar reflectivity, which indicates the amount of precipitation-size hydrometeors (as represented by rain rate) in a given atmospheric layer. We used only nadir observations, which have a resolution of 250 m in the vertical and 4.3 km in the horizontal. Validation of the TRMM PR against high-resolution aircraft and ground-based radar measurements indicates that the instrument performs very well for systems with spatial scales similar to the footprint size (35).

Cloud top pressure, optical depth, and ice-particle effective radius (also referred to here as cirrus particle size) were estimated by using daily gridded data from MODIS (36), onboard Aqua. Because of known biases, particularly the overestimation of ice cloud effective radius (37–40), we considered only the relative size distributions, rather than the absolute values. Last, we used observations of cloud-top pressure from the AIRS (41), also onboard Aqua. The AIRS instrument suite combines soundings from both infrared (AIRS) and microwave (Advanced Microwave Sounding Unit A) instruments to better observe atmospheric profiles. AIRS observes cloud-top pressure by using both sensors at up to two atmospheric levels and with a horizontal resolution of 40.5 km. We used the monthly mean level 3 product (version 4.0.9) in which the orbital observations are assigned to 1° × 1°-grid cells, and an average (weighted by cloud fraction) was computed. Because this product has not yet been validated over land (42), we used it only to further confirm our conclusions from the MLS and MODIS observations.

The large-scale circulation was diagnosed by using version 4.0.4 of the NASA Global Modeling and Assimilation Office meteorological analyses, which provide assimilated data products in nearly real time to support the Earth-observing system Terra, Aqua, and Aura instrument teams and field experiments. The output is resolved on a 1.25° longitude × 1.0° latitude grid at 55 vertical levels in Eta coordinates. The use of Eta coordinates allows the lower atmospheric model layers to be parallel to surface topography. The 6-h averages that were used in this study included surface pressure, temperature, geopotential height, horizontal and vertical winds, potential temperature, and potential vorticity.

Observations of high 100 hPa CO (>80 ppbv) and water vapor (>5 ppmv) are identified in 95 days of MLS data during August to September of 2004 and late July to August of 2005 (version 1.5), corresponding to the period of peak LS hydration (18). The source regions for these observations are then inferred by means of a back-trajectory analysis with the Goddard Fast Trajectory model (43), with a time step of ≈30 min. The model is driven by meteorological fields from the United Kingdom Meteorological Office reanalysis (44), and diabatic heating rates were calculated according to a radiative transfer model (45). For water vapor, the trajectory model was integrated backward in space and time for 3 days; for CO, which has a longer atmospheric residence time, it was integrated for 20 days.

We thank Drs. Anthony Del Genio, Mark Schoeberl, and Peter Webster for insightful comments; Drs. Greg Huey, Michael Bergin, and Paul Wine for helpful discussions; and Dr. Wenhong Li and Susan Ryan for their help with the preparation of the manuscript. This work was supported by the NASA Global Energy and Water Cycle program at the Georgia Institute of Technology and the Aura program at the California Institute of Technology Jet Propulsion Laboratory.

1. Brewer, A. W. (1949) *Q. J. R. Meteorol. Soc.* **75,** 2559–2562.
2. Mote, P. W., Rosenlof, K. H., McIntyre, M. E., Carr, E. S., Gille, J. C., Holton, J. R., Kinnersley, J. S., Pumphrey, H. C., Russell, J. M., III, & Waters, J. W. (1996) *J. Geophys. Res. Atmos.* **101,** 3989–4006.
3. Gettelman, A., Kinnison, D. E., Dunkerton, T. J. & Brasseur, G. P. (August 23, 2004) *J. Geophys. Res. Atmos.*, 10.1029/2004JD004878.
4. Bannister, R. N., O'Neill, A. O., Gregory, A. R. & Nissen, K. M. (2004) *Q. J. R. Meteorol. Soc.* **130,** 1531–1554.
5. Oltmans, S. J. & Hoffman, D. J. (1995) *Nature* **374,** 146–149.
6. Smith, C. A., Toumi, R. & Haigh, J. D. (2000) *Geophys. Res. Lett.* **27,** 585–588.
7. Zhou, X. J., Luo, C., Li, W. L. & Shi, J. E. (1995) *Chinese Sci. Bull.* **4,** 1396–1398.
8. Forster, P. M. de F. & Shine, K. P. (March 22, 2002) *Geophys. Res. Lett.*, 10.1029/2001GL013909.
9. Kirk-Davidoff, D. B., Hintsa, E. J., Anderson, J. G. & Keith, D. W. (1999) *Nature* **402,** 399–401.
10. Li, Q., Jiang, J. H., Wu, D. L., Read, W. G., Livesey, N. J., Waters, J. W., Zhang, Y., Wang, B., Filipiak, M. J., Davis, C. P., *et al.* (June 13, 2005) *Geophys. Res. Lett.*, 10.1029/2005GL022762.
11. Sherwood, S. (2002) *Science* **295,** 1272–1275.
12. Randel, W. J. & Park, M. (2006) *J. Geophys. Res. Atmos.*, in press.
13. Jackson, D. R., Driscoll, S. J., Highwood, E. J., Harries, J. E. & Russell, J. M., III (1998) *Q. J. R. Meteorol. Soc.* **124,** 169–192.
14. Dethof, A., O'Neill, A. & Slingo, J. M. (1999) *Q. J. R. Meteorol. Soc.* **125,** 1079–1106.
15. Dunkerton, T. J. (1995) *J. Geophys. Res. Atmos.* **100,** 16675–16688.
16. Holton, J. R. & Gettelman, A. (2001) *Geophys. Res. Lett.* **28,** 2799–2802.
17. Dessler, A. E. & Sherwood, S. C. (December 2, 2004) *J. Geophys. Res. Atmos.*, 10.1029/2004JD005209.
18. Randel, W. J., III, Zawodny, J. M. & Oltmans, S. J. (2001) *J. Geophys. Res. Atmos.* **106,** 14313–14326.
19. Chen, B. & Liu, X. (January 7, 2005) *Geophys. Res. Lett.*, 10.1029/2004GL020868.
20. Yang, K., Koike, T., Fujii, H., Tamura, T., Xu, X., Bian, L. & Zhou, M. (2004) *J. Meteorol. Soc. Japan* **82,** 1777–1792.
21. Wu, G. X., Li, W., Guo, H., Liu, H., Xue, J. & Wang, Z. (1997) in *Collections on the Memory of Zhao Jiuzhang*, ed. Duzheng, Y. (Chinese Science, Beijing), pp. 116–126.
22. Carrico, C. M., Bergin, M. H., Shrestha, A. B., Dibb, J. E., Gomes, L. & Harris, J. M. (2003) *Atmos. Environ.* **37,** 2811–2824.
23. Hoskins, B. J. (1991) *Tellus* **43AB,** 27–35.
24. Sherwood, S. (2000) *Geophys. Res. Lett.* **27,** 677–680.
25. Gettelman, A. & Forster, P. M. (2002) *J. Meteor. Soc. Japan* **80,** 911–924.
26. McCormack, J. P., Fu, R. & Read, W. G. (2000) *J. Atmos. Sci.* **24,** 241–259.
27. Selkirk, H. B. (1993) *J. Geophys. Res. Atmos.* **98,** 8591–8610.
28. Jensen, E. J., Pfister, L., Ackerman, A. S., Tabazadeh, A. & Toon, O. B. (2001) *J. Geophys. Res. Atmos.* **106,** 17237–17252.
29. Fueglistaler, S., Bonazzola, M., Haynes, P. H. & Peter, T. (January 12, 2005) *J. Geophys. Res. Atmos.*, 10.1029/2004JD005516.
30. Liu, X. & Chen, B. (2000) *Int. J. Climatol.* **20,** 1729–1742.
31. Waters, J. W. (2006) *IEEE Trans. Geosci. Remote Sensing*, in press.
32. Livesey, N. J., Read, W. G., Filipiak, M. J., Froidevaux, L., Harwood, R. S., Jiang, J. H., Jimenez, C., Pickett, H. M., Pumphrey, H. C., Santee, M. L., *et al.* (2005) *Version 1.5 Level 2 Data Quality and Description Document* (Jet Propulsion Laboratory, Pasadena, CA), Technical Report JPL D-32381.
33. Wu, D. L., Jiang, J. H. & Davis, C. P. (2006) *IEEE Trans. Geosci. Remote Sensing*, in press.

34. Kummerow, C., Barnes, W., Kozu, T., Shiue, J. & Simpson, J. (1998) *J. Atmos. Oceanic Technol.* **15,** 809–817.
35. Durden, S. L., Im, E., Haddad, Z. S. & Li, L. (2003) *J. Appl. Meteor.* **42,** 769–774.
36. Platnick, S., King, M. D., Ackerman, S. A., Menzel, W. P., Baum, B. A., Riédi, J. C. & Frey, R. A. (2003) *IEEE Trans. Geosci. Remote Sensing* **41,** 459–473.
37. Rawlins, F. & Foot, J. S. (1990) *J. Atmos. Sci.* **47,** 2488–2504.
38. Nakajima, T., King, M. D., Spinhirne, J. D. & Radke, L. F. (1991) *J. Atmos. Sci.* **48,** 728–751.
39. Kaufman, Y. J. & Nakajima, T. (1993) *J. Appl. Meteor.* **32,** 729–744.
40. Reid, J. S., Hobbs, P. V., Rangno, A. L. & Hegg, D. A. (1999) *J. Geophys. Res. Atmos.* **104,** 6145–6154.
41. Aumann, H. H., Chahine, M. T., Gautier, C., Goldberg, M. D., Kalnay, E., McMillin, L. M., Revercomb, H., Rosenkranz, P. W., Smith, W. L., Staelin, D. H., *et al.* (2003) *IEEE Trans. Geosci. Remote Sensing* **41,** 253–264.
42. Fetzer, E., Eldering, A., Fishbein, E. F., Hearty, T., Irion, W. F. & Kahn, B. (2005) *Validation of AIRS/AMSU/HSB Core Products for Data Release Version 4.0* (Jet Propulsion Laboratory, Pasadena, CA), Technical Report JPL D-31448.
43. Schoeberl, M. R. & Sparling, L. (1995) in *Diagnostic Tools in Atmospheric Physics*: *Proceedings of the International School of Physics Enrico Fermi*, eds. Fiocco, G. & Visconti, G. (IOS, Amsterdam), Vol. 124, pp. 289–306.
44. Swinbank, R. & O Niell, A. (1994) *Mon. Weather Rev.* **122,** 686–702.
45. Rosenfield, J. E., Newman, P. A. & Schoeberl, M. R. (1994) *J. Geophys. Res. Atmos.* **99,** 16677–16689.